BELYAKOV HOMOCLINIC BIFURCATIONS IN A TRITROPHIC FOOD CHAIN MODEL *

YU.A. KUZNETSOV†, O. DE FEO‡, AND SERGIO RINALDI§

Abstract. Complex dynamics of the most frequently used tritrophic food chain model are investigated in this paper. First it is shown that the model admits a sequence of pairs of Belyakov bifurcations (codimension-two homoclinic orbits to a critical node). Then fold and period-doubling cycle bifurcation curves associated to each pair of Belyakov points are computed and analyzed. The overall bifurcation scenario explains why stable limit cycles and strange attractors with different geometries can coexist. The analysis is conducted by combining numerical continuation techniques with theoretical arguments.

Key words. homoclinic bifurcations, population dynamics, continuation.

AMS subject classifications. 34C37, 58F13, 92D25.

1. Introduction. For several decades, after the pioneering work of Lotka [34] and Volterra [42], one of the topics of major concern in mathematical ecology has been the study of ditrophic food chains. This has been accomplished by analyzing a great number of second-order continuous-time dynamical models, usually called prey–predator models (see, for example [2]). Existence of limit cycles, multiplicity of attractors and catastrophic bifurcations are the characteristics of those models which have been used to explain complex behaviors observed in the field. It is only in the late seventies that some interest in the mathematics of tritrophic food chain models (composed of prey, predator, and top-predator) emerged. With almost no exception, the first contributions dealt with the problem of persistence [18, 19, 17] and, therefore, did not provide information on the number and the geometry of the attractors. This is a very unfortunate situation because the nature of the attractors is often the most interesting feature of a dynamical system. An exception in this respect was an almost unnoticed paper [25], where it was shown through simulation that a particular food chain model can behave chaotically. This property was in practice brought to the attention of the scientific community by a contribution [24] that appeared much later and showed that food chains behave chaotically on a "tea-cup" strange attractor provided the three populations have diversified time responses increasing from bottom to top. This condition on the time responses was used in the same years [38, 39] to perform a singular perturbation analysis that indeed confirms that the tea-cup geometry is the result of the interactions between high frequency (prey–predator) oscillations and low frequency (predator–top-predator) oscillations. Since then, particular effort has been devoted to the study of the complex dynamics of food chain systems and bifurcation analysis has been the major tool of investigation.

*This work has been supported by Consiglio Nazionale delle Ricerche, Italy, Project ST/74 "Mathematical models and methods for the study of biological phenomena". The second authors gratefully acknowledges financial support from the Swiss National Science Foundation: 2000-056030.98.

†Mathematical Institute, Utrecht University, Budapestlaan 6, P.O. Box 80010, 3508 TA Utrecht, The Netherlands; and Institute of Mathematical Problems of Biology, Russian Academy of Sciences, Pushchino, Moscow Region, 142290 Russia. E-mail: kuznet@math.uu.nl.

‡ Laboratory of Nonlinear Systems (DSC-LANOS), Swiss Federal Institute of Technology Lausanne (EPFL), 1015 Lausanne, Switzerland.

§ Dipartimento di Elettronica e Informazione, Politecnico di Milano, Via Ponzio 34/5, 20133 Milano, Italy.

The most recent studies [28, 37, 33, 11, 5] dealing with the so-called Rosenzweig-MacArthur model show that its bifurcation structure is quite rich. In particular, it comprises a complex cascade of tangent bifurcations of cycles intersecting with flip bifurcation curves, thus delimiting a region of very complex behavior, sometimes called the *chaotic region* [33]. Although these analyses were restricted to local bifurcations, they clearly indicate the presence of global bifurcations. Indeed, *homoclinic orbits*, *i.e.*, orbits tending toward the same saddle equilibrium or saddle cycle forward and backward in time, have been numerically detected in [37, 33, 5] and even proved to exist through singular perturbation analysis in the case of trophic levels with time responses increasing from bottom to top [12]. Similar analysis have been performed on more complex food chain models [4, 23, 30, 40] and the results are qualitatively the same: Homoclinic orbits exist and very complex behavior is possible.

Despite the efforts devoted to the analysis of the Rosenzweig-MacArthur food chain model, a systematic study of its chaotic region has not yet been attempted. The aim of this paper is to accomplish this study by combining recent numerical techniques for continuing homoclinic bifurcations [6, 7] with the analysis of a special codim-2 homoclinic bifurcation first studied in [3] and here referred to as *Belyakov bifurcation*. In particular, it will be shown that a number of homoclinic bifurcation curves exists in a two parameter space and that two Belyakov points are located on each of these curves. Since the original analysis in [3] was insufficient for our purposes, we have revisited Belyakov's proofs and have shown that three families of subsidiary bifurcation curves (namely, *tangent*, *flip*, and *double homoclinic*) are rooted at each Belyakov point. These points are therefore the *organizing centers* of the overall bifurcation scenario. Another organizing feature of the two-parameter bifurcation diagram is the sharp turn of the primary homoclinic curves.

The paper is structured as follows. In the next section some background information on the Rosenzweig-MacArthur model is given, while in Sect. 3 the simplest local bifurcations relative to equilibria and cycles are discussed. Then, in Sect. 4, the bifurcation structure of the chaotic region is discussed in detail. The basic properties of the Belyakov homoclinic points are presented in Appendix, where the asymptotic expressions for the subsidiary bifurcation curves are derived.

The authors would like to thank Dr. A.J. Homburg (University of Amsterdam) for useful discussions on Belyakov points.

2. The Model and Its Equilibria. The model we analyze in this paper describes a tritrophic food chain composed of a logistic prey (X), a Holling type II predator (Y) and a Holling type II top-predator (Z). It is, therefore, given by the following system of ordinary differential equations (see [24] for more details):

$$\frac{dX}{dT} = X\left[R\left(1-\frac{X}{K}\right) - \frac{A_1 Y}{B_1+X}\right], \tag{2.1a}$$

$$\frac{dY}{dT} = Y\left[E_1\frac{A_1 X}{B_1+X} - \frac{A_2 Z}{B_2+Y} - D_1\right], \tag{2.1b}$$

$$\frac{dZ}{dT} = Z\left[E_2\frac{A_2 Y}{B_2+Y} - D_2\right], \tag{2.1c}$$

where T is time, R and K are prey intrinsic growth rate and carrying capacity, the A_i's are maximum predation rates, the B_i's are half saturation constants, the D_i's are death rates and the E_i's are efficiencies of predator ($i = 1$) and top-predator ($i = 2$). In order to preserve the biological meaning of the model the parameters are

assumed strictly positive. Furthermore, to avoid the case where predator and top-predator cannot survive, even when their food is infinitely abundant, we assume that $E_iA_i > D_i,\ i = 1, 2$.

By rescaling the variables,

$$x_1 = X,\ x_2 = \frac{Y}{E_1},\ x_3 = \frac{Z}{E_1E_2},\ t = T,$$

one obtains

$$\frac{dx_1}{dt} = x_1\left[r\left(1 - \frac{x_1}{K}\right) - \frac{a_1x_2}{1 + b_1x_1}\right], \tag{2.2a}$$

$$\frac{dx_2}{dt} = x_2\left[\frac{a_1x_1}{1 + b_1x_1} - \frac{a_2x_3}{1 + b_2x_2} - d_1\right], \tag{2.2b}$$

$$\frac{dx_3}{dt} = x_3\left[\frac{a_2x_2}{1 + b_2x_2} - d_2\right], \tag{2.2c}$$

where

$$r = R,\ a_1 = \frac{A_1E_1}{B_1},\ b_1 = \frac{1}{B_1},\ d_1 = D_1,\ a_2 = \frac{A_2E_1E_2}{B_2},\ b_2 = \frac{E_1}{B_2},\ d_2 = D_2.$$

Then, the above conditions for predator and top-predator persistence become $a_i > b_id_i,\ i = 1, 2$.

The reference parameter values used in this paper are those used in [33], namely

$$a_1 = 5,\ a_2 = 0.1,\ b_1 = 3,\ b_2 = 2,\ d_1 = 0.4,\ d_2 = 0.01,$$

while the two remaining parameters K and r are varied to perform the bifurcation analysis. The reader interested in the biological interpretation of these parameter values can refer to [36].

All coordinate axes and faces of the positive orthant are invariant sets of system (2.2). There are three trivial equilibria:

- the origin $(0, 0, 0)$, which is always a saddle;
- the point $(K, 0, 0)$, corresponding to prey at carrying capacity and absence of predator and top-predator;
- the point

$$x^{(0)} = \left(x_1^{(0)}, x_2^{(0)}, 0\right) = \left(\frac{d_1}{a_1 - b_1d_1},\ \frac{r\left[a_1 - d_1\left(b_1 + \frac{1}{K}\right)\right]}{(a_1 - b_1d_1)^2},\ 0\right), \tag{2.3}$$

  which is positive for $a_1 > d_1\left(b_1 + \frac{1}{K}\right)$ and corresponds to prey–predator coexistence and absence of top-predator.

The point $x^{(0)}$ can be either stable or unstable in the face (x_1, x_2). When it is unstable, it is surrounded by a stable limit cycle [35], which is unique and globally attracting in the plane $x_3 = 0$ [9]. The transition between the two situations corresponds to a supercritical Hopf bifurcation of the submodel (2.2a-2.2b) with $x_3 = 0$ and occurs for

$$Kb_1\left(a_1 - b_1d_1\right) = a_1 + b_1d_1. \tag{2.4}$$

Moreover, a second degeneracy of the point $x^{(0)}$ occurs when the term in the square brackets of (2.2c) annihilates, namely when

$$r\left(a_2 - b_2d_2\right)\left(K\left(a_1 - b_1d_1\right) - d_1\right) = d_2K\left(a_1 - b_1d_1\right)^2. \tag{2.5}$$

It is a transcritical bifurcation giving rise to a strictly positive equilibrium for small perturbations of the parameters.

As for nontrivial equilibria, it is possible to show that at most two of them can be positive, namely:

$$x^{(1)} = \left(x_1^{(1)}, x_2^{(1)}, x_3^{(1)}\right) = (\beta_1, \alpha, \gamma_1)\,, \tag{2.6}$$

$$x^{(2)} = \left(x_1^{(2)}, x_2^{(2)}, x_3^{(2)}\right) = (\beta_2, \alpha, \gamma_2)\,, \tag{2.7}$$

where

$$\alpha = \frac{d_2}{a_2 - b_2 d_2}, \tag{2.8a}$$

$$\beta_{1,2} = \frac{1}{2}\left[K - \frac{1}{b_1} \pm \sqrt{\left(K + \frac{1}{b_1}\right)^2 - 4\frac{K}{r}\frac{a_1}{b_1}\alpha}\right], \tag{2.8b}$$

$$\gamma_{1,2} = \frac{(1 + b_2\alpha)\,(a_1 - b_1 d_1)\left(\beta_{1,2} - \dfrac{d_1}{a_1 - b_1 d_1}\right)}{a_2\,(1 + b_1\beta_{1,2})}. \tag{2.8c}$$

Depending upon the parameter values, there are three possible cases: none of these equilibria is strictly positive, only $x^{(1)}$ is strictly positive or both $x^{(1)}$ and $x^{(2)}$ are strictly positive. When $x^{(2)}$ is positive it is always a repeller, while $x^{(1)}$ can be either an attractor or a saddle.

3. Bifurcations of Equilibria and Local Bifurcations of Limit Cycles.

3.1. Codimension-two point M. If all parameters, except K and r, are fixed, the planar Hopf bifurcation (2.4) and the transcritical bifurcation of equilibria (2.5) occur along two curves in the (K, r)-plane, labeled by H_p and TC_e in FIG. 3.1. These curves intersect at a codimension-two point M with coordinates

$$M = (K_M, r_M) = \left(\frac{1}{b_1}\frac{a_1 + b_1 d_1}{a_1 - b_1 d_1},\ \frac{d_2}{a_1}\frac{a_1^2 - (b_1 d_1)^2}{a_2 - b_2 d_2}\right)$$

and the coordinates (see (2.3)) of the corresponding equilibrium point $x_M^{(0)}$ (with one zero eigenvalue and two purely imaginary eigenvalues) are

$$x_M^{(0)} = \left(x_{1M}^{(0)}, x_{2M}^{(0)}, x_{3M}^{(0)}\right) = \left(\frac{d_1}{a_1 - b_1 d_1},\ \frac{d_2}{a_2 - b_2 d_2},\ 0\right)$$

The analysis of the bifurcations in the vicinity of $x_M^{(0)}$ for parameter values close to (K_M, r_M) can be performed using the normal form technique [1]. In particular, a parameter-dependent normal form of the system near this point has been derived and used to show [33] that five bifurcation curves emerge from this point. None of these curves implies chaos, so that the codimension-two point M can not be considered as the "origin" of chaos in food chains, as first argued in [28].

3.2. Bifurcation curves rooted at point M. The bifurcation curves emerging from point M have been continued numerically using LOCBIF [27], see FIG. 3.1. The curve H_p is a vertical straight line because r is not present in eq. (2.4); the curve T_e is

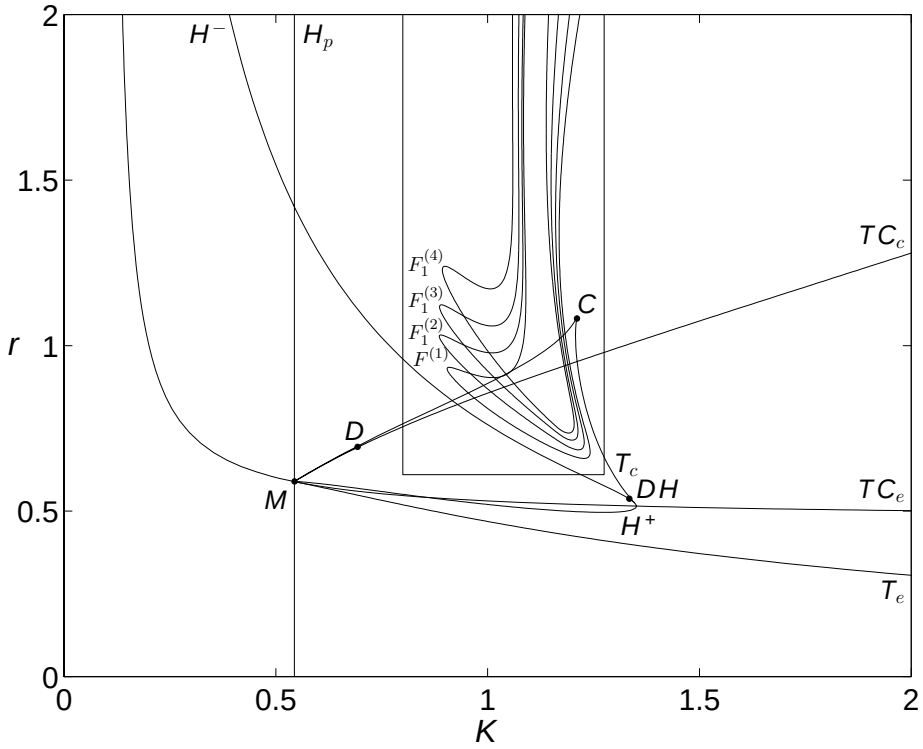

FIG. 3.1. *Some local bifurcation curves of system* (2.2) *in the* (K, r)*-plane*: H_p *– Hopf bifurcation in the plane* $x_3 = 0$; TC_e *– transcritical bifurcation of equilibrium* $x^{(0)}$; TC_c *– transcritical bifurcation of cycle*; $H^{\pm}$ *and* T_e *– Hopf and tangent bifurcations of positive equilibria*; T_c *– tangent bifurcation of limit cycles*; $F^{(1)}$ *and* $F_1^{(i)}$ *– flip bifurcations of limit cycles. Codimension two bifurcation points:* M *– zero-Hopf bifurcation in the plane* $x_3 = 0$; DH *– degenerate Hopf bifurcation*; C *– cusp bifurcation of limit cycles*; D *– degenerate transcritical bifurcation of limit cycles.*

the tangent bifurcation curve for equilibria, where $x^{(1)}$ and $x^{(2)}$ collide and disappear (annihilation of the radical in eq. (2.8b)); TC_e is a transcritical bifurcation curve of equilibria (see eq. (2.5)), where a strictly positive equilibrium emerges from point $x^{(0)}$; TC_c is a transcritical bifurcation curve for cycles, where a strictly positive limit cycle emerges from the limit cycle in the plane (x_1, x_2); finally, the curve $H = H^+ \cup H^-$ is a Hopf bifurcation curve. Crossing curve H^-, the equilibrium $x^{(1)}$ looses its stability and a stable limit cycle appears around it. By contrast, crossing curve H^+, the equilibrium $x^{(1)}$ looses its stability while an unstable cycle shrinks on it. The first Lyapunov coefficient associated with the Hopf bifurcation H (*i.e.*, the real part of the cubic coefficient in the normal form [31]) is positive close to M and decreases from M to DH, where it vanishes. This means that the Hopf bifurcation is subcritical from M to DH (segment H^+) and supercritical elsewhere (segment H^-). Therefore (see, for example, [31]) there exists a tangent bifurcation of limit cycles T_c originating at point DH and corresponding to the collision of two positive limit cycles. Numerical continuation shows that curve T_c has a second codimension two singularity, namely a cusp C, where three limit cycles collide simultaneously. The curve T_c terminates at a point D on the transcritical bifurcation curve TC_c, where a cycle passes through the invariant plane $x_3 = 0$: when approaching point D along T_c, the two colliding cycles

"hit" the invariant face. Thus, the curve T_c connects the codimension-two bifurcation points DH and D.

3.3. Cascades of flip bifurcations. The bifurcation curves described so far form a bifurcation set connected with point M. However, the actual bifurcation diagram is much more complex and involves many other bifurcation curves that are disconnected from the previous ones. Figure 3.1 shows four such curves $F^{(1)}$, $F_1^{(2)}$, $F_1^{(3)}$ and $F_1^{(4)}$, computed with LOCBIF [27] and AUTO97 [14]. These curves are part of a bifurcation scenario, composed of Feigenbaum-like (period-doubling) cascades alternated with chaotic windows. The continuation for decreasing values of K, of the stable limit cycle existing in the right-upper corner of FIG. 3.1, reveals a flip bifurcation curve $F^{(1)}$ followed by a Feigenbaum's cascade of flips $F_1^{(2)}, F_2^{(2)}, F_3^{(2)}, \ldots$ ending with a curve $F_\infty^{(2)}$ after which the attractor is a strange attractor. Notice that only the first flip $F_1^{(2)}$ of this Feigenbaum's cascade is shown in FIG. 3.1. The chaotic region delimited on the right by $F_\infty^{(2)}$ ends, on the left, with an "attractor crisis", namely with the sudden disappearance of the strange attractor, which is substituted by a period-3 cycle, namely by a cycle characterized by three prey–predator oscillations per cycle, *i.e.*, by three minima of the prey x_1 per cycle (see FIG. 3.2). Decreasing K further,

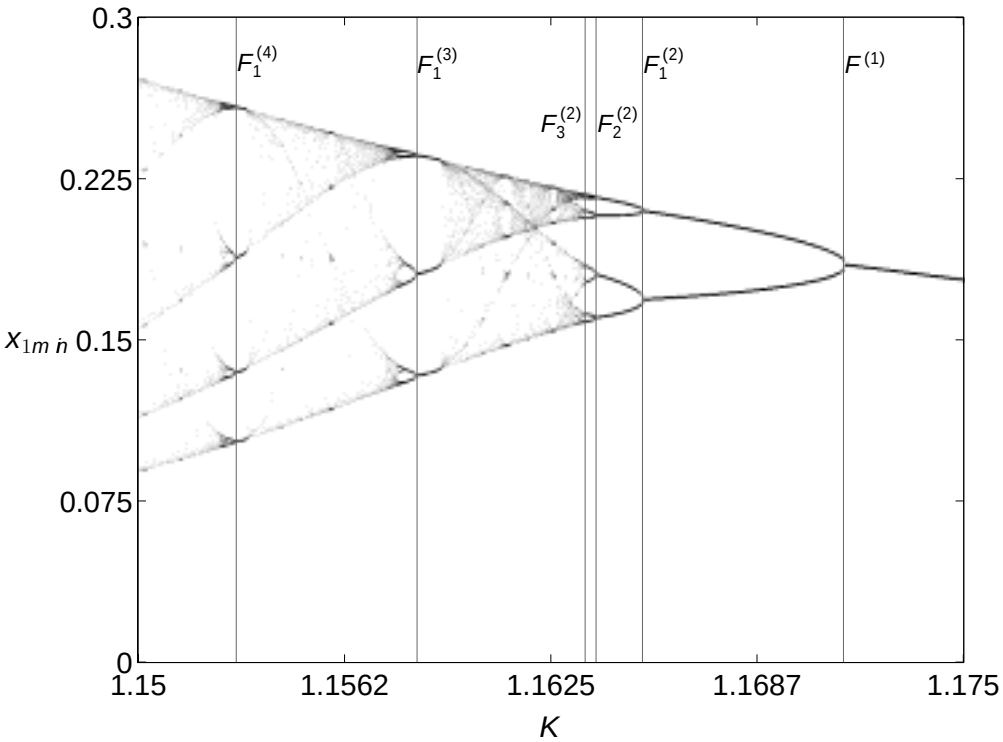

FIG. 3.2. *One parameter bifurcation scenario with respect to K for the cycle existing in the right-upper corner of* FIG. 3.1 ($r = 1.2$).

the period-3 periodic window ends with the flip bifurcation $F_1^{(3)}$ shown in Figs. 3.1 and 3.2. Such a bifurcation is the first period-doubling of a new Feigenbaum's cascade $F_1^{(3)}, F_2^{(3)}, F_3^{(3)}, \ldots$ ending at $F_\infty^{(3)}$, where a new strange attractor appears. And the

story repeats: The second chaotic region is followed by a period-4 periodic window, which is then interrupted by the flip curve $F_1^{(4)}$ which is the first period-doubling of a Feigenbaum's cascade $F_1^{(4)}, F_2^{(4)}, F_3^{(4)}, \ldots F_\infty^{(4)}$. Figure 3.2 shows that the attractors (cycles and strange attractors) of the system are obtained from "generating cycles" through a series of bifurcations, and that each generating cycle is characterized by a different number i of prey–predator oscillations, namely by a different number i of minima of the prey (x_1) per cycle.

It will be shown later that the generating cycles organize the overall bifurcation structure. This is why a superscript $^{(i)}$ will characterize all bifurcation curves. For example, the k-th flip bifurcation of the period-i generating cycle is called $F_k^{(i)}$. There is, however, a hidden drawback in such notations, since the number i could change in the continuation (see below).

Coming back to Fig. 3.1, we can notice that the left side of the chaotic region is quite complex, because on that side the flip curves intersect one with each other (and with other bifurcation curves not shown in the figure). This problem will be studied in the next section by focusing on the rectangular subregion indicated in Fig. 3.1.

4. Homoclinic Orbits and Associated Bifurcations. We show in this section that limit cycle bifurcations characterizing the chaotic region are organized by an infinite family of U-shaped bifurcation curves $h^{(i)}$, $i = 1, 2, \ldots$, corresponding to the presence of orbits homoclinic to the saddle (or saddle-focus) $x^{(1)}$. For simplicity, the first one of these bifurcation curves is called *primary* and all the others *secondary*. We can anticipate that each homoclinic bifurcation corresponds to homoclinic orbits that differ in the number of minima of the prey. These bifurcation curves are computed using the numerical toolbox for homoclinic bifurcation analysis HomCont [6, 7] incorporated into Auto97 [14]. It turns out that when the equilibrium $x^{(1)}$ is a saddle-focus its complex-conjugate eigenvalues have positive real part and are closer to the imaginary axis than the real eigenvalue, so that Shilnikov's theorem [31] implies the existence of an infinite number of saddle limit cycles for parameter values near the homoclinic bifurcation curves. As shown in [21, 15, 22, 20], under the same conditions at least three countable families of subsidiary bifurcations (flip, tangent, and homoclinic) accumulate on each homoclinic curve. Moreover, two Belyakov points, *i.e.*, two codim-2 homoclinic bifurcation points where the transition from saddle-focus to saddle of the equilibrium occurs, lie on each homoclinic bifurcation curve and are the roots of the subsidiary bifurcations. Finally, the geometry of the subsidiary bifurcation curves is determined by the sharp U-turn of the homoclinic curves $h^{(i)}$.

All these facts imply that the chaotic region has a very complex structure and is actually fractalized in regions where chaotic attractors coexist with cycles with different numbers of prey–predator oscillations per cycle.

4.1. Primary homoclinic and subsidiary bifurcations. Through the numerical continuation in (K, r) of the flip curve $F^{(1)}$ (see Fig. 3.1), one can easily discover that the period of the cycle becomes very large on the left branch of the curve when r becomes slightly bigger than 4. This is a clear indication that the cycle is very close to a homoclinic orbit. Further simulations, combined with suitable perturbations of the parameters, allow one to detect a homoclinic bifurcation point with an associated homoclinic orbit characterized by a single minimum of the prey. Then, through the two-parameter continuation, an entire homoclinic bifurcation curve $h^{(1)}$ can be produced. Such a curve is U-shaped, as qualitatively sketched in Fig. 4.1. For sufficiently high values of r the right branch of $h^{(1)}$ corresponds to homoclinic orbits

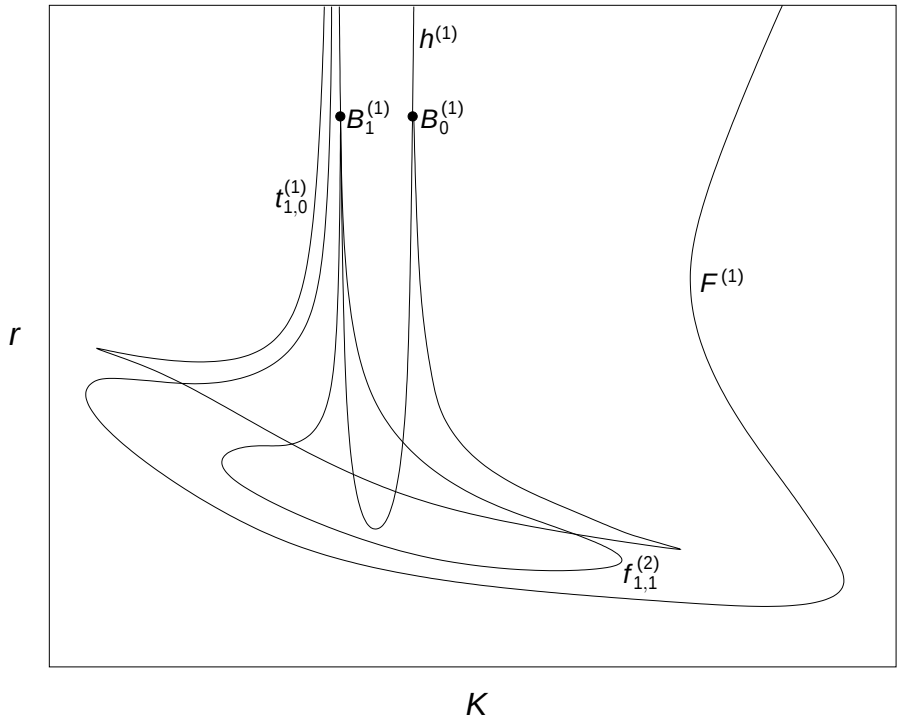

FIG. 4.1. *Sketch of bifurcation curves associated with the first Belyakov pair* $B_0^{(1)}$ *and* $B_1^{(1)}$*:* $h^{(1)}$ *– primary homoclinic bifurcation;* $t_{1,0}^{(1)}$ *– tangent bifurcation of limit cycles;* $F^{(1)}$ *and* $f_{1,1}^{(2)}$ *– flip bifurcations of limit cycles. The upper index* $^{(i)}$ *indicates the number of prey–predator oscillations per cycle.*

to a saddle with a single minimum of the prey. Going down along the right branch we pass the first Belyakov point $B_0^{(1)}$ ($K = 1.2202954903...$, $r = 4.0263103008...$) and below that point we have homoclinic orbits to a saddle-focus. Proceeding further, after a turning point we encounter the second Belyakov point $B_1^{(1)}$, after which we have again homoclinic orbits to a saddle. While making the U-turn, the geometry of the homoclinic orbit changes significantly because a second minimum of the prey appears, namely the homoclinic orbit makes then two global turns involving two oscillations of the prey–predator subsystem. Figure 4.2 shows how the homoclinic orbits vary along the bifurcation curve $h^{(1)}$. The homoclinic orbits associated to the right branch of $h^{(1)}$ have a single prey–predator oscillation while those associated to the left branch have two oscillations.

It has been proved in [3] that each Belyakov point is the origin of two infinite families of subsidiary bifurcation curves. One is a family of tangent bifurcations of cycles and the other is a family of homoclinic bifurcations associated to homoclinic orbits (called *double*) characterized by a number of global turns which is twice that of the primary homoclinic orbit. We prove in the Appendix that an infinite family of flip bifurcation curves is also rooted there. All these curves accumulate exponentially fast on the primary homoclinic curve $h^{(1)}$ and have infinite-order tangency to it at the Belyakov point. These accumulation properties are so strong that it is very difficult to numerically produce more than a few of these subsidiary curves. In the present case

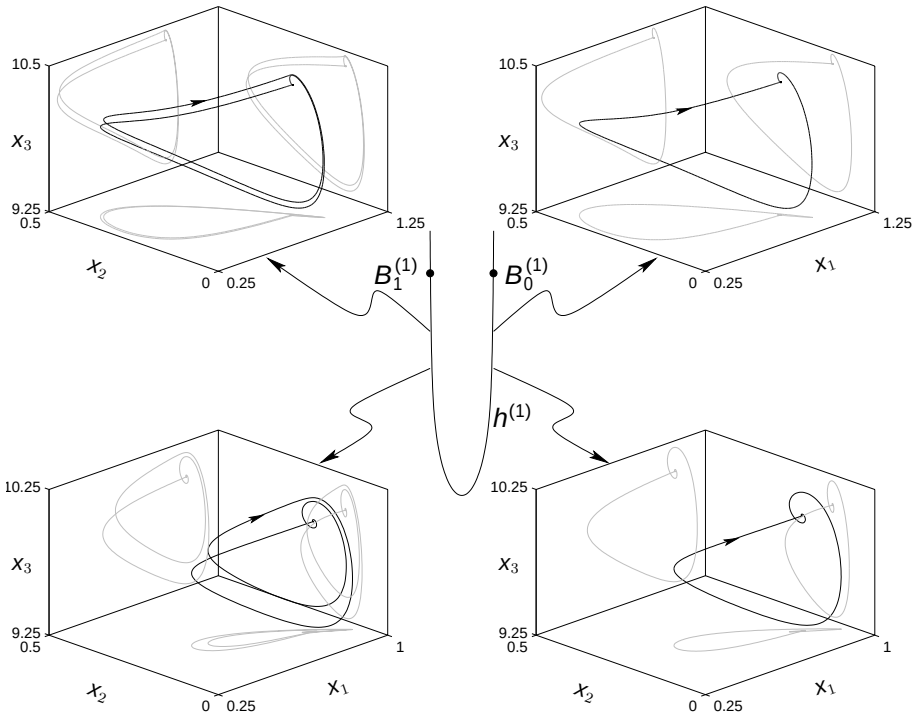

FIG. 4.2. *Deformation of the homoclinic orbit along the curve $h^{(1)}$: the homoclinic orbits associated to the right [left] branch of $h^{(1)}$ have one minimum [two minima] of $x_1(t)$.*

we were able to compute (through continuation) only the first tangent and the first flip bifurcation curve of the corresponding families, as sketched in FIG. 4.1. The tangent bifurcation $t_{1,0}^{(1)}$ starts from point $B_0^{(1)}$ and has two cusps, while the flip bifurcation $f_{1,1}^{(2)}$ starts and returns to the same Belyakov point $B_1^{(1)}$. Note that the cycles associated to these bifurcation curves have one and two minima of the prey per cycle and this is why the curves are identified with the superscripts $^{(1)}$ and $^{(2)}$, respectively. In reality the U-turn is very sharp (as noticed in [30] for a similar model) and the two Belyakov points almost coincide. However, it is possible to distinguish them by zooming on the corresponding homoclinic orbits in the vicinity of the saddle equilibrium $x^{(1)}$, as shown in FIG. 4.3. Moreover, the four bifurcation curves $F^{(1)}$, $h^{(1)}$, $t_{1,0}^{(1)}$ and $f_{1,1}^{(2)}$ shown in FIG. 4.1 practically coincide in the vicinity of the Belyakov points, while the flip curve $F^{(1)}$ is well separated from $h^{(1)}$.

In conclusion, the bifurcation diagram associated to the primary homoclinic $h^{(1)}$ is composed of $h^{(1)}$ itself, of the subsidiary bifurcations $f_{i,0}^{(1)}$, $t_{i,0}^{(1)}$, and $h_{i,0}^{(1)}$, $i = 1, 2, \ldots$, associated with $B_0^{(1)}$ and of the subsidiary bifurcations $f_{i,1}^{(2)}$, $t_{i,1}^{(2)}$, and $h_{i,1}^{(2)}$, $i = 1, 2, \ldots$, associated with $B_1^{(1)}$. These results are in agreement with the two-parameter analysis performed in [20], where, nevertheless, the sharp geometry of the homoclinic curve was not fully understood, since homoclinic orbits with two global turns were not even taken into account. Figure 4.4 shows the partial bifurcation diagram we were able to obtain: at that scale the two Belyakov points appear as a single point and the two branches of the primary homoclinic are not distinguishable.

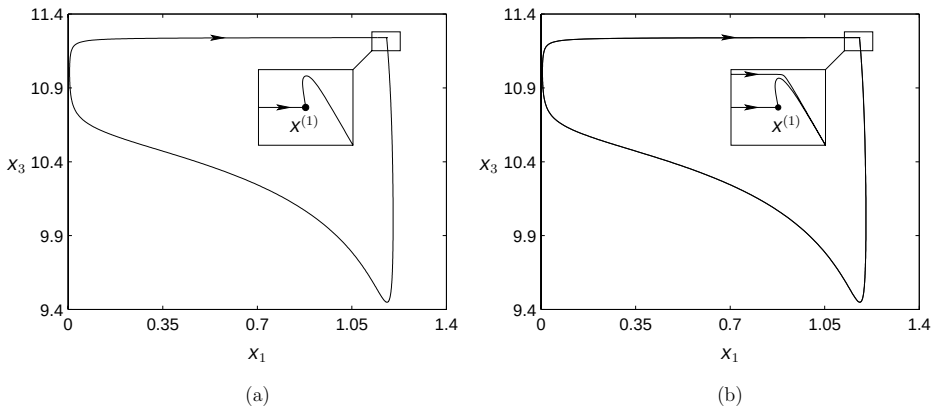

FIG. 4.3. *Resolution of the Belyakov points by zooming on the equilibrium* $x^{(1)}$: (a) – $B_0^{(1)}$; (b) – $B_1^{(1)}$.

4.2. Secondary homoclinics and subsidiary bifurcations. The bifurcation diagrams associated to the secondary homoclinics $h^{(2)}$, $h^{(3)}$, ... have the same structure than the diagram associated to the primary homoclinic $h^{(1)}$. The homoclinic orbits associated to the homoclinic bifurcation curves $h^{(i)}$ involve i or $(i+1)$ minima of the prey per cycle, instead of one or two. Figure 4.5 shows a qualitative sketch of the diagram associated to $h^{(2)}$. The homoclinic bifurcation curve $h^{(2)}$ is U-shaped and has two Belyakov points $B_0^{(2)}$ and $B_1^{(2)}$. The homoclinic orbits associated to the right branch of $h^{(2)}$ make two global turns, while those associated to the left branch make three global turns, as clearly detectable in FIG. 4.6, where the homoclinic orbits at the Belyakov points are shown. Notice that, these two orbits are more easily distinguishable than in the case of the primary homoclinic $h^{(1)}$.

The main difference between the bifurcation scenario associated with the primary homoclinic (FIG. 4.1) and the scenario associated with the secondary homoclinics (FIG. 4.5) is that in the last one a tangent bifurcation curve $t_{0,1}^{(3)}$ rooted at the left Belyakov point $B_1^{(2)}$ is also present. As in the primary case, the two Belyakov points are so close to appear as a single point, as shown in FIG. 4.7, reporting actual results of our computations. At the scale of the figure, the two branches of $h^{(2)}$ cannot be distinguished and the bifurcation curves $h^{(2)}$, $f_{1,1}^{(3)}$, $t_{0,1}^{(3)}$ and $t_{1,0}^{(2)}$ appear as a single curve in the vicinity of the Belyakov points. The flip $F_1^{(2)}$ tends asymptotically to $t_{1,0}^{(2)}$ as r increases.

The same results can be obtained for a few other secondary homoclinic curves $h^{(i)}$. Indeed, we have been able to perform the computations up to the fifth homoclinic bifurcation $h^{(5)}$. Superimposing the five corresponding diagrams we have obtained the bifurcation subset shown in FIG. 4.8.

In such a diagram the ten Belyakov points appear as a single point and the five homoclinic curves $h^{(i)}, i = 1, \ldots, 5$ can be hardly distinguished. By contrast, the subsidiary bifurcation curves $t_{1,0}^{(i)}$, $t_{0,1}^{(i+1)}$, $f_{1,1}^{(i+1)}$, $F_1^{(i)}$ can be fairly well identified. Nevertheless, we like to stress that these curves represent only a very small fraction of the complete bifurcation set. First of all, because each one of these curves is only one representative of an infinite family of similar bifurcation curves and, second, because the subsidiary homoclinic curves are missing since we were unable to produce them

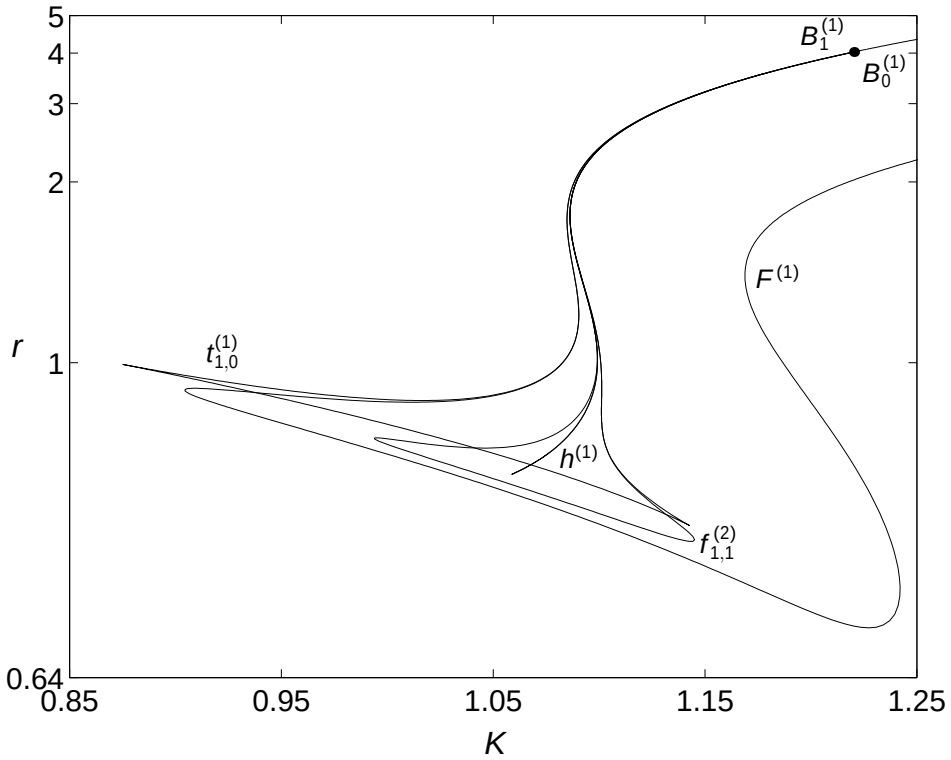

FIG. 4.4. *Computed bifurcation curves associated with the first Belyakov pair. Labelling as in* FIG. 4.1. *The two Belyakov points* $B_0^{(1)}$ *and* $B_1^{(1)}$ *are indistinguishable at this scale.*

numerically. Moreover, we must also mention that there are other global bifurcations involved such as the recently discovered [5] heteroclinic bifurcations, concerning orbits connecting the saddle point $x^{(1)}$ to a saddle limit cycle.

5. Discussion. We have shown in the previous sections (see, in particular, FIG. 4.8) that a family of homoclinic bifurcations organize the structure of the so called chaotic region. This region is fractalized in subregions of chaotic and/or periodic behavior and the coexisting attractors (cycles and strange attractors) are characterized by different geometries, namely by a different number of prey–predator oscillations. The coexistence of different attractors is due to the overlapping of the basic bifurcation structures sketched in Figs. 4.1 and 4.5. The series of Feigenbaum-like cascades that exists on the right side of the chaotic region is also organized by the same bifurcation structure. Indeed, the curves $t_{0,1}^{(i+1)}$ and $F_1^{(i)}$ on the right of FIG. 4.8 form the skeleton of the series of Feigenbaum's cascades described in Sect. 3.3 and in FIG. 3.2. In fact, the curve $t_{0,1}^{(i+1)}$ is the tangent bifurcation that opens the periodic window of period-$(i+1)$ and the curve $F_1^{(i+1)}$ is the first flip of the period-$(i+1)$ cycle.

In order to show how the attractors depend upon K and r we have plotted in FIG. 5.1 the period T of the cycle born on the Hopf bifurcation curve H^- of FIG. 3.1. The period T has been computed through continuation with respect to r for different values of K. The points marked with a triangle are flip points, while those marked with a circle are tangent points, and the number of prey–predator oscillations

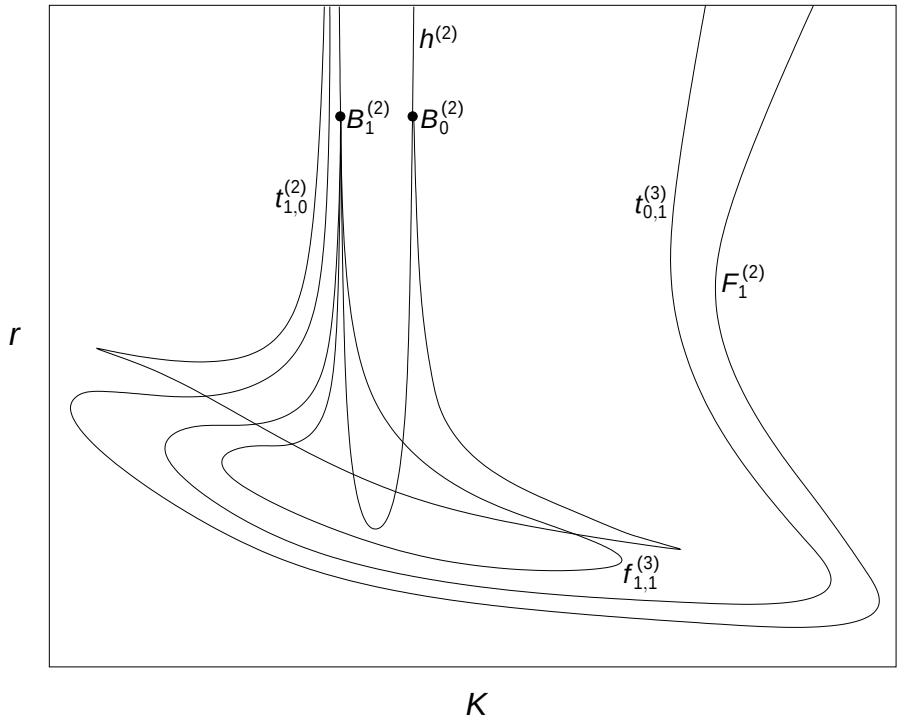

FIG. 4.5. *Sketch of bifurcation curves associated with the second Belyakov pair* $B_0^{(2)}$ *and* $B_1^{(2)}$*:* $h^{(2)}$ *– secondary homoclinic bifurcation;* $t_{1,0}^{(2)}$ *and* $t_{0,1}^{(3)}$ *– tangent bifurcations of limit cycles;* $F_1^{(2)}$ *and* $f_{1,1}^{(3)}$ *– flip bifurcations of limit cycles. The upper index* $^{(i)}$ *indicates the number of prey oscillations per cycle.*

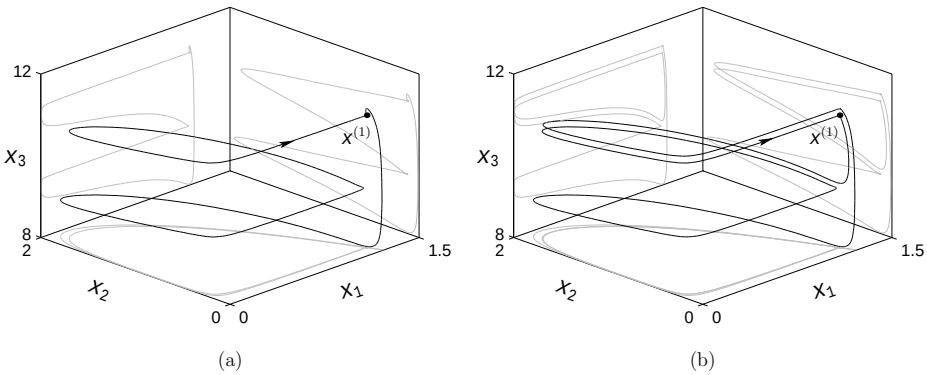

FIG. 4.6. *Homoclinic orbits corresponding to the Belyakov points:* (a) – $B_0^{(2)}$; (b) – $B_1^{(2)}$.

present in each cycle is indicated within parentheses. Moreover, FIG. 5.2 reports, for four different values of K, the bifurcation scenarios of the minima of x_1 on the attractors. Each scenario is accompanied by the two parameters bifurcation diagram in the neighborhood of the K value characterizing the scenario.

For $K < 0.87$, *i.e.*, when the bifurcations of FIG. 4.8 are not involved, there exists only one stable cycle. Its period T, as well as the number of prey–predator oscillations,

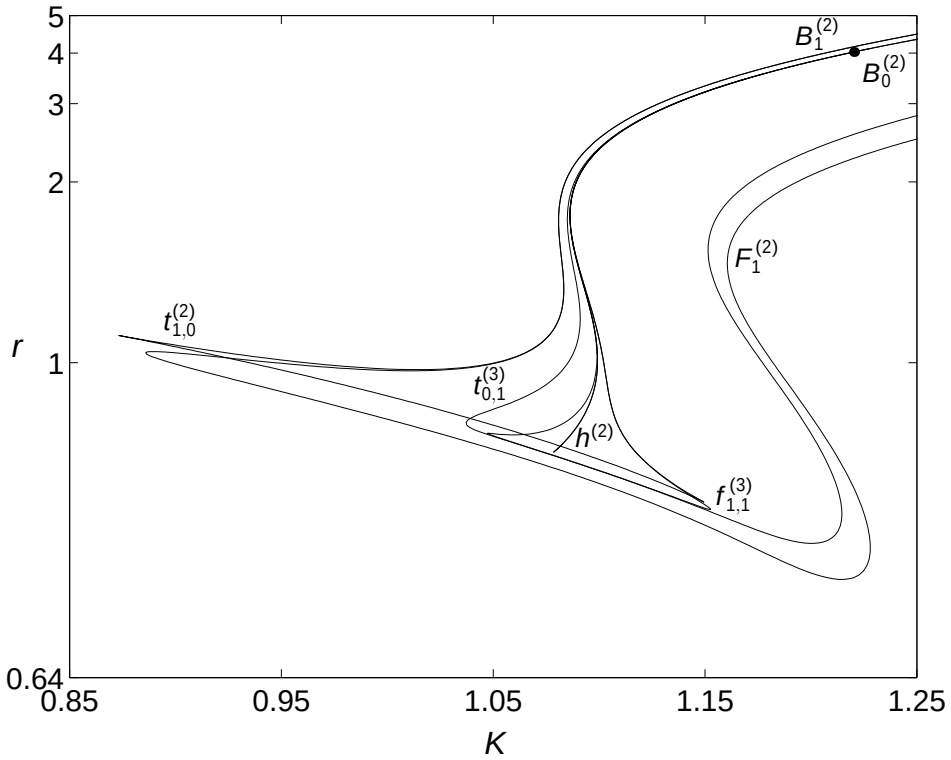

FIG. 4.7. *Computed bifurcation curves associated with the second Belyakov pair. Labelling as in* FIG. 4.1.

increases with r as indicated in FIG. 5.1. Consistently, FIG. 5.2(a), obtained for $K = 0.85$, shows that there is only one cycle and that the number of minima of x_1 per cycle increases from 1 to 5 in the interval $0.9 \leq r \leq 1.6$. The values of r at which the number of minima of x_1 changes are values for which the periodic function $x_1(t)$ has an inflection point with $\dot{x}_1 = 0$. The locus where these inflections occur is reported in the two parameter bifurcation diagram with a dotted line.

For $0.87 < K < 1.05$, *i.e.*, from the first overlapping of flip and tangent bifurcation curves to the (primary and secondary) homoclinic bifurcation curves $h^{(1)}, h^{(2)}, \ldots$ (see FIG. 4.8), the period T of the cycle and the number of global turns still increase with r (see FIG. 5.1) but coexistence of different attractors with different number of global turns per cycle is possible. The bifurcation scenario of FIG. 5.2(b), obtained for $K = 0.96$, clearly points out this possibility.

For $1.05 < K < 1.17$, *i.e.*,from the homoclinic bifurcations $h^{(i)}$ to the end of the flip and tangent overlapping (see again FIG. 4.8), the number of global turns of $x_1(t)$ per cycle still increases with r while the period T of the cycle increases and decreases alternatively (see FIG. 5.1). The scenario in FIG. 5.2(c) shows that the previous well organized structure is no longer present and that the minima of x_1 in the strange attractor do not belong to separated segments. This means that the geometry of the strange attractor is no longer simple.

Finally, for $K > 1.17$, *i.e.*, when there are no flip and tangent overlapping (see FIG. 4.8), a series of Feigenbaum's cascades alternated with chaotic windows can be

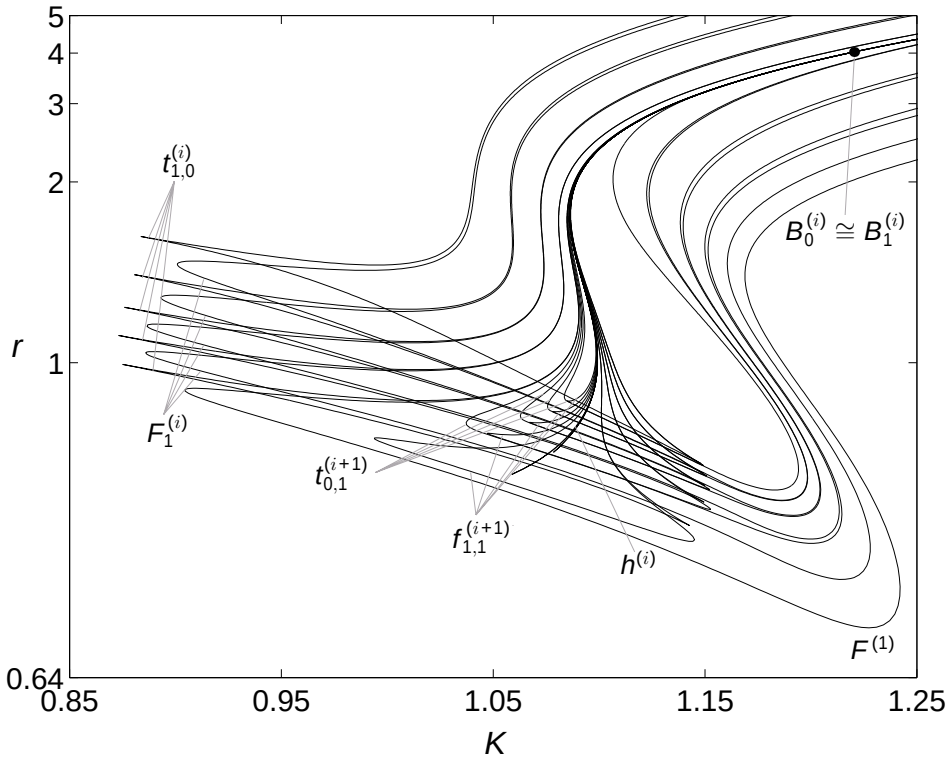

FIG. 4.8. *Detailed bifurcation structure of the chaotic region.*

observed (see FIG. 5.2(d)). The fact that there is also a series of reversed Feigenbaum's cascades is due to the curvature of the flip and tangent bifurcations.

All the results we have found through continuation are in agreement with simulation experiments which are summarized in FIG. 5.3. In this figure more intense gray levels are associated with more complex attractors characterized by higher numbers of prey–predator oscillations. The figure clearly shows that the right side of the chaotic region is regularly organized in bands of simple and complex attractors. By contrast, the left side of the chaotic region is fractalized in subregions with simple and complex behaviors. The figure also points out the existence of an island of simple behavior inside the chaotic region. This island, first discovered in [40], has been recently shown to be related to heteroclinic orbits to a saddle cycle [5].

6. Concluding Remarks. We have studied in this paper the most common model of tritrophic food chains by focusing on its local and global bifurcations. We have discovered that the models has an infinite number of homoclinic bifurcation curves and that on each one of them there are two special points, namely, codim-2 Belyakov homoclinic bifurcation points. We have proved that three infinite families of subsidiary (flip, tangent and homoclinic) bifurcation curves emerge from each Belyakov point. The numerical computation of these subsidiary bifurcations and the analysis of their intertwining has allowed us to understand the structure of the so called chaotic region. In particular, we have discovered that the number of oscillations per cycle of one of the three state variables turns out to be a useful complexity

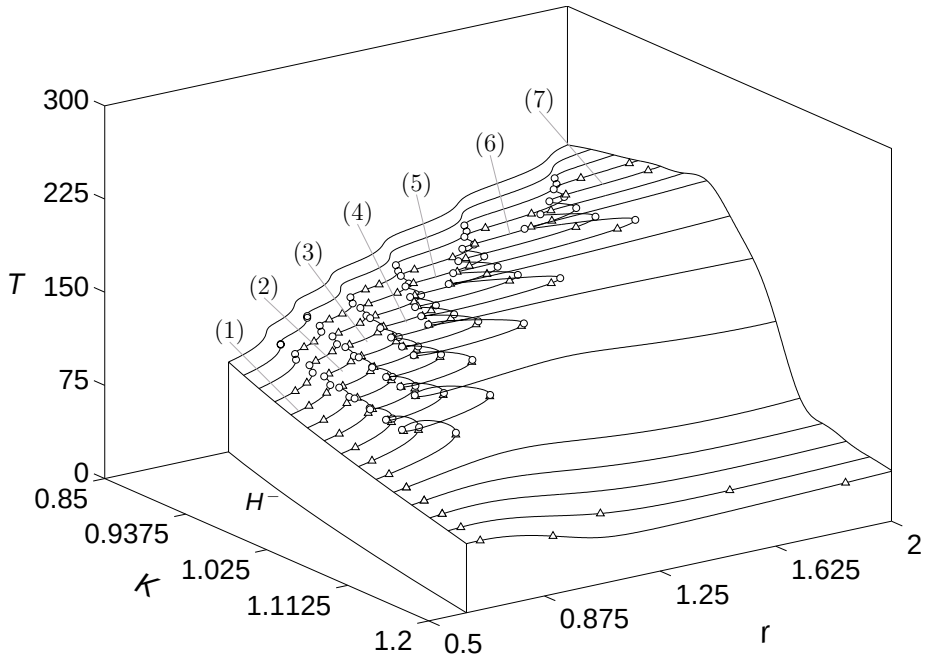

FIG. 5.1. *The period T of the cycles in the chaotic region: circles and triangles represent tangent and flip bifurcations, respectively.*

index for encoding the attractors, and that one side of the chaotic region is nicely organized in bands of alternate high and low complexity, while the other side is completely fractalized in terms of complexity.

From a theoretical point of view, our analysis is interesting because it contains new results concerning flip bifurcation curves near Belyakov points (*cf.*, [3]). Moreover, the basic bifurcation scenario near the U-turn of each homoclinic curve (see FIG. 4.1 and FIG. 4.5) adds some details to the results described in [20], in particular about homoclinic orbits with several global turns. But our study is also interesting from the computational point of view because it shows how powerful the combination of theoretical analysis and continuation techniques can be for understanding the behavior of nonlinear dynamical systems.

The results pointed out in this paper can be interpreted biologically by noticing that one of the two parameters of our discussion, namely the prey carrying capacity K, can be controlled through enrichment or impoverishment of the habitat of the prey population. In particular, our analysis shows that the dynamic complexity of the ecosystem first increases and then decreases with enrichment. This result is particularly interesting because extensive simulations of the same model have pointed out [11] that in the case when the top-predator is harvested at constant effort, also the mean yield first increases and then decreases with enrichment and reaches its maximum roughly on the right border of the chaotic region. We can therefore hope that our results can be used for proving this important and intriguing property of exploited renewable resources.

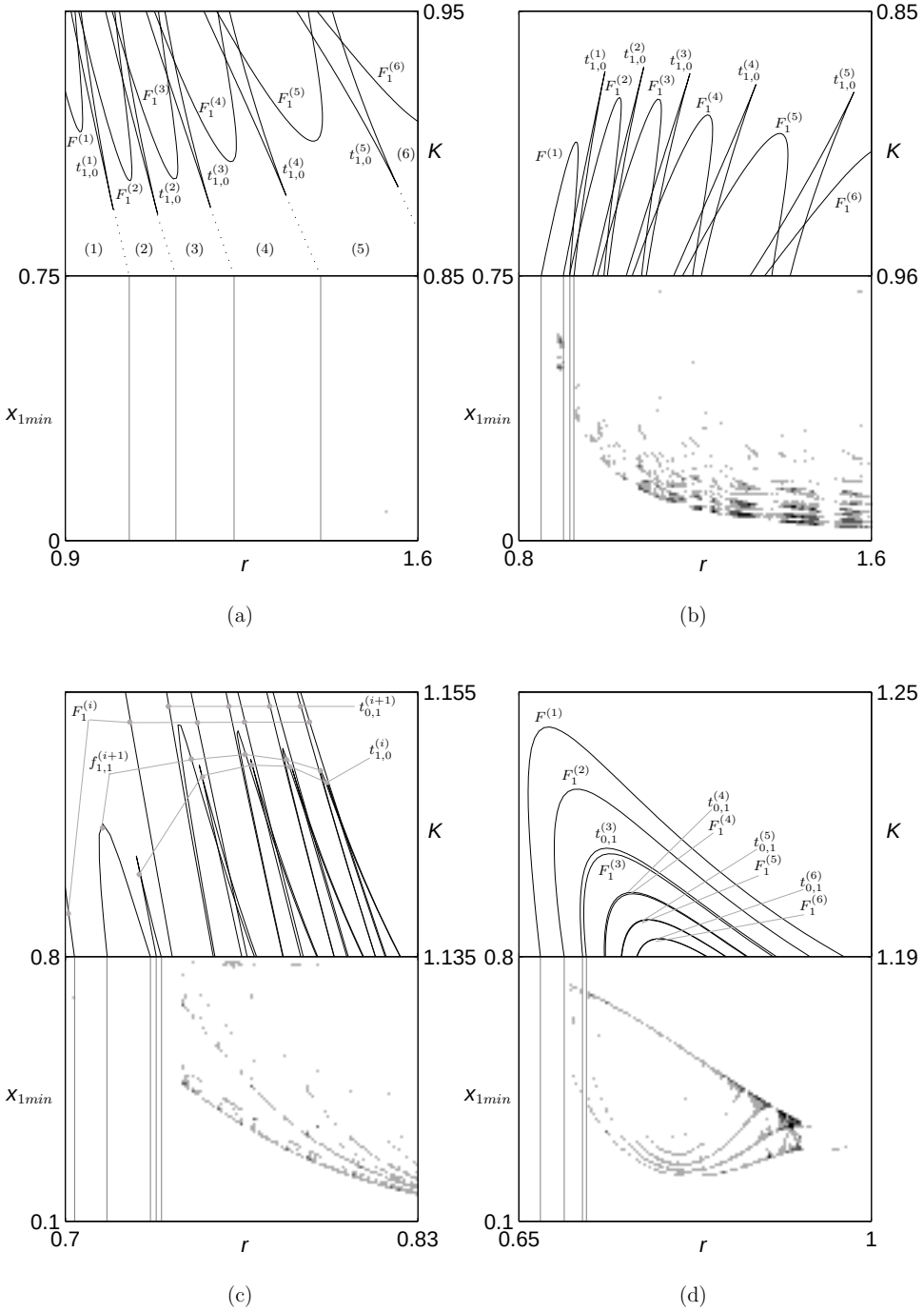

FIG. 5.2. *Bifurcation diagrams in subregions of the chaotic region and bifurcation scenarios of* x_{1min} *with respect to* r *for four values of* K : (a) – $K = 0.85$; (b) – $K = 0.96$; (c) – $K = 1.135$; (d) – $K = 1.19$.

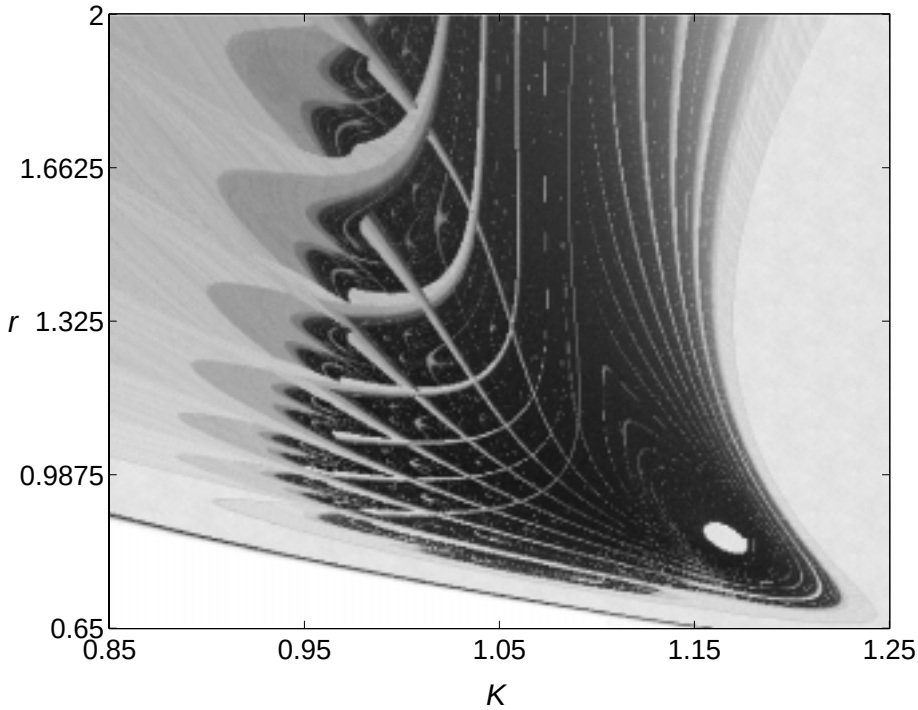

FIG. 5.3. *Experimental two-parameter bifurcation diagram showing the complexity of the attractors. Intense gray levels correspond to attractors with a high number of prey–predator oscillations.*

Finally, we like to mention that the study we have performed in this paper could be repeated for a variety of different but similar models that have been used to describe various phenomena, like alternation between despotism and anarchy in ancient China [16], electrical activity of pancreatic cells [8, 41], microbial dynamics in the chemostat [29], autocatalytic enzymatic reactions [13, 26], and the use of electronic oscillators as chaos generators for communication and artificial intelligence purposes [10].

Appendix A. Belyakov Bifurcation Revisited. In this Appendix we apply the scaling techniques from [22] to analyze subsidiary bifurcations near the Belyakov point. The resulting analysis is simpler but more complete than the one in the original paper [3]. Namely, the following theorem will be proved.

THEOREM A.1. *Consider a generic smooth three-dimensional system of ordinary differential equations depending upon two parameters, having at some parameter values a homoclinic orbit* Γ_1 *to an equilibrium* O *with eigenvalues* $\lambda_{1,2} = \gamma_0 < 0$, $\lambda_3 = \nu_0 > -\gamma_0$. *Then the corresponding point in the parameter plane is the origin of three countable sets of subsidiary bifurcation curves, namely*:

(1) $t_n^{(1)}$ – *tangent bifurcation curves of periodic orbits making one global passage near* Γ_1;
(2) $f_n^{(1)}$ – *flip bifurcation curves of periodic orbits making one global passage near* Γ_1;
(3) $h_n^{(2)}$ – *bifurcation curves, corresponding to the existence of saddle-focus homoclinic orbits making two global passages near* Γ_1.

The curves $t_n^{(1)}$ *and* $f_n^{(1)}$ *accumulate exponentially fast at both sides on the saddle-*

focus part of a bifurcation curve $h^{(1)}$ corresponding to the existence of a homoclinic orbit to the equilibrium making one global passage near $,_1$, while the curves $h_n^{(2)}$ do so at one side only. The orbits corresponding to the curves with bigger integer $n \in \mathbb{N}$ make more local turns near the equilibrium before the global passage.

The theorem is illustrated in Fig. A.1. The existence of the flip bifurcation curves was not reported in [3], although probably known to the experts. It should be noted that there are many other bifurcation curves in a neighborhood of the Belyakov point, corresponding, for example, to *triple homoclinic loops*. Moreover, such homoclinic curves may be not rooted at the Belyakov point [22].

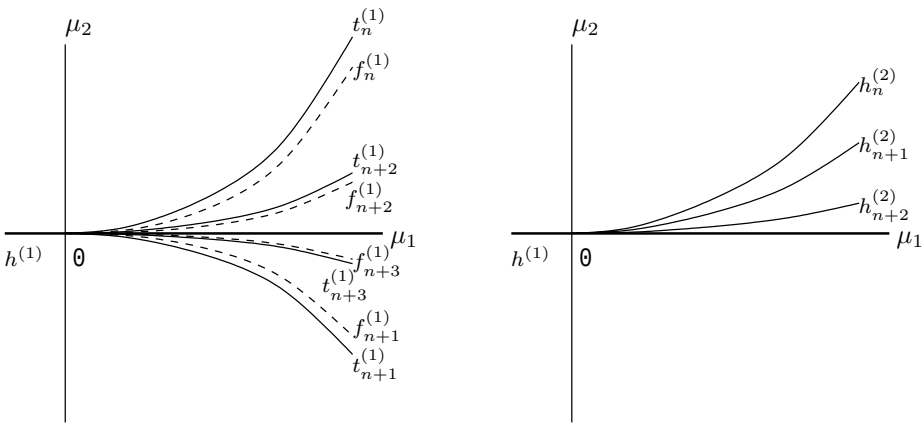

Fig. A.1. *Bifurcation curves rooted at the Belyakov point: $t_n^{(1)}$ – primary tangent bifurcation curves, $f_n^{(1)}$ – primary flip bifurcation curves, $h^{(1)}$ and $h_n^{(2)}$ – primary and secondary (double) homoclinic bifurcation curves.*

A.1. New coordinates and parameters. Any generic system satisfying the theorem's conditions can be transformed near the critical parameter values ($\mu = 0$), in a neighborhood of the equilibrium O, to the form:

$$\text{(A.1)} \qquad \begin{cases} \dot{x} &= \gamma(\mu)x + y + f_1(x,y,z,\mu)x + f_2(x,y,z,\mu)y, \\ \dot{y} &= -\mu_1 x + \gamma(\mu)y + g_1(x,y,z,\mu)x + g_2(x,y,z,\mu)y, \\ \dot{z} &= \lambda(\mu)z, \end{cases}$$

where $\mu = (\mu_1, \mu_2)^T$ are small parameters, the smooth functions $\gamma(\mu)$ and $\lambda(\mu)$ satisfy $\gamma(0) = \gamma_0 < 0$, $\lambda(0) = \nu_0 > 0$, while $f_{1,2}$ and $g_{1,2}$ are smooth functions of their arguments. The transformation to the form (A.1) is achieved by smooth coordinate and parameter changes and by a time reparametrization [3]. At $\mu = 0$, the system (A.1) has a *critical node* O at $x = y = z = 0$ with eigenvalues

$$\lambda_{1,2} = \gamma(0), \ \lambda_3 = \lambda(0).$$

For $\mu_1 < 0$, the eigenvalues of the equilibrium O are real and simple, while for $\mu_1 > 0$ there is a simple pair of complex-conjugate eigenvalues and a positive eigenvalue.

For all sufficiently small $\|\mu\|$, the equilibrium O has a one-dimensional unstable manifold $W^u(O)$ composed of two outgoing orbits, $,_1$ and $,_2$, and a two-dimensional stable manifold $W^s(O)$ composed of all incoming orbits (see Fig. A.2). In the co-

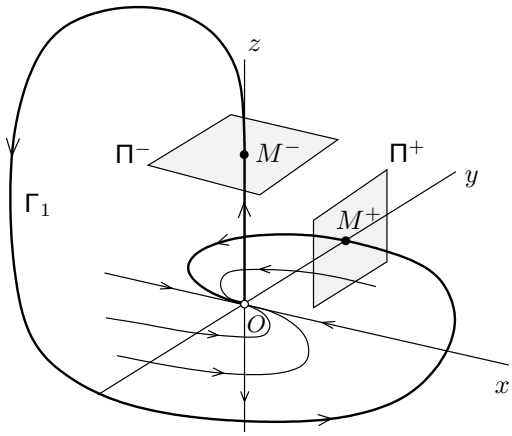

FIG. A.2. *Homoclinic orbit to a critical node at the Belyakov bifurcation. Local planar sections* $\Pi^{\pm}$ *are transverse to the homoclinic orbit* Γ_1 *at points* $M^{\pm}$.

ordinates (x, y, z), the manifold $W^u(O)$ locally coincides with the z-axis, while the manifold $W^s(O)$ is locally represented by $z = 0$. Let Γ_1 depart from the equilibrium O along the positive half of the z-axis.

By the theorem's conditions, at $\mu = 0$ the system (A.1) has a homoclinic orbit: Γ_1 returns to the equilibrium O. Generically, upon return, it does not coincide with the x-axis. Also generically, Γ_1 misses the stable manifold $W^s(O)$ near O by the μ_2-shift in the z-direction, when $\mu_2 \neq 0$. This means, in particular, that for all $|\mu_1|$ small and $\mu_2 = 0$ the system (A.1) has a homoclinic orbit to O: It is homoclinic to the saddle for $\mu_1 < 0$ and to the saddle-focus for $\mu_1 > 0$.

Our aim is to analyze the bifurcation diagram of (A.1) for small $\|\mu\|$ in the half-plane $\mu_1 > 0$ in the Shil'nikov case:

$$\lambda(0) > -\gamma(0). \tag{A.2}$$

In the opposite case the bifurcation behavior of (A.1) is rather simple: A unique stable limit cycle bifurcates from the homoclinic orbit for $\mu_2 > 0$. In both cases, crossing the line $\mu_2 = 0$ when $\mu_1 < 0$ results in the appearance of a single limit cycle.

A.2. Poincaré map. The technique to analyze the behavior of (A.1) near the bifurcation is rather standard and consists of reducing its analysis to that of a Poincaré map near the homoclinic orbit.

Let $M^- = (0, 0, z^-)$, respectively $M^+ = (0, y^+, 0)$, be a point at the departing, respectively incoming, part of the homoclinic orbit Γ_1 at $\mu = 0$. We introduce two local cross-sections to Γ_1 at these points: $\Pi^-(x_1, y_1, z^-)$ and $\Pi^+(0, y_0, z_0)$ (see Figure A.2). Here the pairs of coordinates (y_0, z_0) and (x_1, y_1) are used to parameterize the cross-sections. As usual, the Poincaré map $P : \Pi^+ \to \Pi^+$ along orbits of the system can be defined for all small $\|\mu\|$ as a product of the *singular map* $\Delta : \Pi^+ \to \Pi^-$ (near the equilibrium O) and the *regular map* $Q : \Pi^- \to \Pi^+$ (near the global part of the homoclinic orbit):

$$P = Q \circ \Delta.$$

The singular map Δ, that is mainly determined by the linear part of (A.1), has the

form

$$x_1 = \frac{y_0}{\sqrt{\mu_1}} \left(\frac{z_0}{z^-}\right)^\rho \sin\left(-\frac{\sqrt{\mu_1}}{\lambda} \ln \frac{z_0}{z^-}\right) + o\left(\left(\frac{z_0}{z^-}\right)^\rho\right),$$
$$y_1 = y_0 \left(\frac{z_0}{z^-}\right)^\rho \cos\left(-\frac{\sqrt{\mu_1}}{\lambda} \ln \frac{z_0}{z^-}\right) + o\left(\left(\frac{z_0}{z^-}\right)^\rho\right),$$

where

$$\rho = -\frac{\gamma}{\lambda} < 1. \tag{A.3}$$

The rescaling

$$\frac{x_1}{y^+} \mapsto x_1, \ \frac{y_0}{y^+} \mapsto y_0, \ \frac{z_0}{z^-} \mapsto z_0,$$

brings Δ to the form

$$\Delta : \left\{ \begin{array}{lcl} x_1 & = & \frac{1}{\sqrt{\mu_1}} y_0 z_0^\rho \sin\left(-\frac{\sqrt{\mu_1}}{\lambda} \ln z_0\right) + o(z_0^\rho), \\ y_1 & = & y_0 z_0^\rho \cos\left(-\frac{\sqrt{\mu_1}}{\lambda} \ln z_0\right) + o(z_0^\rho). \end{array} \right. \tag{A.4}$$

The regular map Q, which is a diffeomorphism, can be written in the rescaled coordinates in the form

$$Q : \left\{ \begin{array}{lcl} y_0 & = & 1 + a x_1 + b y_1 + O(x_1^2 + y_1^2), \\ z_0 & = & \mu_2 + c x_1 + d y_1 + O(x_1^2 + y_1^2), \end{array} \right. \tag{A.5}$$

where a, b, c, and d are smooth functions of μ such that $a(0)d(0) - b(0)c(0) \neq 0$.

Taking the product of the maps Δ and Q, defined respectively by (A.4) and (A.5), we get

$$y_0' = 1 + \frac{a}{\sqrt{\mu_1}} y_0 z_0^\rho \cos\left(-\frac{\sqrt{\mu_1}}{\lambda} \ln z_0 + \Psi\right) + o\left(\frac{z_0^\rho}{\sqrt{\mu_1}}\right),$$
$$z_0' = \mu_2 + \frac{b}{\sqrt{\mu_1}} y_0 z_0^\rho \sin\left(-\frac{\sqrt{\mu_1}}{\lambda} \ln z_0 + \Phi\right) + o\left(\frac{z_0^\rho}{\sqrt{\mu_1}}\right),$$

where Ψ and Φ are functions of μ, namely,

$$\cos\Psi = \frac{b}{a}\sqrt{\mu_1} + o(\sqrt{\mu_1}), \quad \sin\Phi = -\frac{d}{b}\sqrt{\mu_1} + o(\sqrt{\mu_1}).$$

Finally, the substitution

$$z_0 \mapsto z_0 \exp\left(\frac{\lambda\Phi}{\sqrt{\mu_1}}\right), \quad \mu_2 \mapsto \mu_2 \exp\left(-\frac{\lambda\Phi}{\sqrt{\mu_1}}\right),$$

brings the Poincaré map P to the form:

$$P : \left\{ \begin{array}{lcl} y_0' & = & 1 + \frac{A}{\sqrt{\mu_1}} y_0 z_0^\rho \cos\left(-\frac{\sqrt{\mu_1}}{\lambda} \ln z_0 + \Theta\right) + o\left(\frac{z_0^\rho}{\sqrt{\mu_1}}\right), \\ z_0' & = & \mu_2 + \frac{B}{\sqrt{\mu_1}} y_0 z_0^\rho \sin\left(-\frac{\sqrt{\mu_1}}{\lambda} \ln z_0\right) + o\left(\frac{z_0^\rho}{\sqrt{\mu_1}}\right), \end{array} \right. \tag{A.6}$$

with Θ being some function depending on μ, and

$$A = a \exp\left(-\frac{\rho\lambda d}{b}\right), \quad B = b \exp\left(-\frac{(\rho-1)\lambda d}{b}\right).$$

A.3. Tangent and flip curves. A fixed point (y, z) of (A.6) satisfies the system

$$\begin{cases} y &= 1 + \frac{A}{\sqrt{\mu_1}} y z^\rho \cos\left(-\frac{\sqrt{\mu_1}}{\lambda}\ln z + \Theta\right) + o\left(\frac{z^\rho}{\sqrt{\mu_1}}\right), \\ z &= \mu_2 + \frac{B}{\sqrt{\mu_1}} y z^\rho \sin\left(-\frac{\sqrt{\mu_1}}{\lambda}\ln z\right) + o\left(\frac{z^\rho}{\sqrt{\mu_1}}\right). \end{cases}$$

Applying the Implicit Function Theorem to the first equation in a neighborhood of $y = 1,\ z = 0$, we get

$$y = 1 + O\left(\frac{z^\rho}{\sqrt{\mu_1}}\right).$$

Thus, the z-component of the fixed point satisfies the scalar equation

$$z = \mu_2 + \frac{B}{\sqrt{\mu_1}} z^\rho \sin\left(-\frac{\sqrt{\mu_1}}{\lambda}\ln z\right) + o\left(\frac{z^\rho}{\sqrt{\mu_1}}\right),$$

or

$$z = G(z, \mu) + o\left(\frac{z^\rho}{\sqrt{\mu_1}}\right), \tag{A.7}$$

where

$$z \mapsto G(z, \mu) = \mu_2 + \frac{B}{\sqrt{\mu_1}} z^\rho \sin\left(-\frac{\sqrt{\mu_1}}{\lambda}\ln z\right). \tag{A.8}$$

Tangent bifurcations of the fixed points in (A.6) correspond to double roots of (A.7), i.e.

$$1 = G_z(z, \mu) + o\left(\frac{z^{\rho-1}}{\sqrt{\mu_1}}\right), \tag{A.9}$$

whose leading term coincides with the tangent bifurcation condition for the map (A.8). Similarly, one can see that flip bifurcations of the fixed points in (A.6) happen when

$$-1 = G_z(z, \mu) + o\left(\frac{z^{\rho-1}}{\sqrt{\mu_1}}\right). \tag{A.10}$$

Also in this case, the leading term coincides with that of the flip bifurcation condition for the map (A.8). For this reason we call (A.8) the *normal form* for the Belyakov bifurcation.

Due to assumption (A.3), equation (A.7) has countably many roots near the origin ($z = 0$), which can be isolated by writing

$$-\frac{\sqrt{\mu_1}}{\lambda}\ln z = \pi n + \theta, \tag{A.11}$$

where $n \in \mathbb{N}$ is sufficiently big and $\theta \in \left[-\frac{\pi}{2}, \frac{\pi}{2}\right)$. Having in mind (A.11), *both* tangent condition (A.9) and flip condition (A.10) can be rewritten in terms of (θ, n) as

$$0 = \rho\sin\theta - \frac{\sqrt{\mu_1}}{\lambda}\cos\theta + O\left(\mathrm{e}^{-\frac{n}{\sqrt{\mu_1}}}\right).$$

Therefore, due to (A.3),

$$\theta = -\frac{\sqrt{\mu_1}}{\gamma} + o(\sqrt{\mu_1}).$$

By substituting this expression into the fixed point equation (A.7) and by taking into account (A.11), we obtain the following asymptotic representation for the tangent bifurcation curve:

$$\mu_2 = \frac{(-1)^n B}{\mathrm{e}\gamma} \mathrm{e}^{\frac{\gamma \pi n}{\sqrt{\mu_1}}} [1 + \beta_1(\mu_1)], \tag{A.12}$$

where $\beta_1(\mu_1) \to 0$ as $\mu_1 \to 0$. Thus, there is a countable set of *tangent bifurcation curves* $t_n^{(1)}$ of (A.8), accumulating on the primary homoclinic curve $h^{(1)}$ ($\mu_2 = 0$) for small $\mu_1 > 0$. All these curves have infinite-order tangency with that curve at $\mu_1 = 0$.

Since the leading terms of the tangent and flip bifurcation conditions coincide, (A.12) also gives (with another $\beta_1(\mu_1)$) a representation of the flip bifurcation curves $f_n^{(1)}$ near the origin ($\mu = 0$). This has been noticed in a different context in [20]. Therefore, the Belyakov point is also the origin of a countable set of the *flip bifurcation curves* $f_n^{(1)}$ which have the same properties as $t_n^{(1)}$.

A.4. Secondary homoclinic curves. The point M^- of the intersection of $,_1$ with the plane Π^- has the coordinates $(x_1, y_1) = (0, 0)$ and is mapped by the global map Q (see (A.5)) into a point $M_1 = Q(M^-) \in \Pi^+$ with the coordinates $(y_0, z_0) = (1, \mu_2)$. If the image point $M_2 = P(M_1)$ returns to the stable manifold of O, i.e. its z-coordinate happens to be zero, we have a *double homoclinic orbit* (see Fig. A.3). Therefore, the bifurcation condition for (A.1) to have a double homoclinic

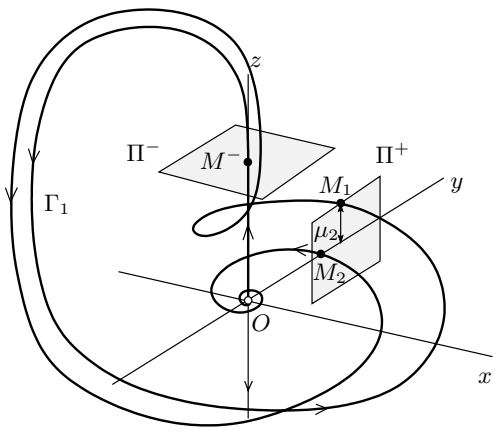

Fig. A.3. *Double homoclinic loop to a saddle-focus near the Belyakov bifurcation:* $M_2 \in W^s(O)$.

orbit to O can now be expressed using (A.6) as

$$0 = \mu_2 + \frac{B}{\sqrt{\mu_1}} {\mu_2}^{\rho} \sin\left(-\frac{\sqrt{\mu_1}}{\lambda} \ln \mu_2\right) + o\left(\frac{{\mu_2}^{\rho}}{\sqrt{\mu_1}}\right). \tag{A.13}$$

Provided (A.3) is true, this equation defines countably many functions representing the *double homoclinic bifurcation curves* $h_n^{(2)}$ for small $\mu_1 > 0$. Indeed, writing

$$-\frac{\sqrt{\mu_1}}{\lambda} \ln \mu_2 = \pi n + \theta, \tag{A.14}$$

where $n \in \mathbb{N}$ is sufficiently big and $\theta \in \left[-\frac{\pi}{2}, \frac{\pi}{2}\right)$, it follows from (A.14) and (A.13) that

$$\exp\left(-\frac{(\lambda+\gamma)}{\sqrt{\mu_1}}(\pi n+\theta)\right) = \frac{(-1)^{n+1}B}{\sqrt{\mu_1}}\sin\theta + \ldots,$$

which gives

$$\theta = (-1)^{n+1}\left(\frac{\sqrt{\mu_1}}{B}\mathrm{e}^{-\frac{(\lambda+\gamma)\pi n}{\sqrt{\mu_1}}} + \ldots\right).$$

Substituting this expression back into (A.13) using (A.14), we get the following asymptotic expression for the double homoclinic bifurcation curves:

$$\mu_2 = \mathrm{e}^{-\frac{\lambda\pi n}{\sqrt{\mu_1}}}[1+\beta_2(\mu_1)], \tag{A.15}$$

where $\beta_2(\mu_1) \to 0$ as $\mu_1 \to 0$.

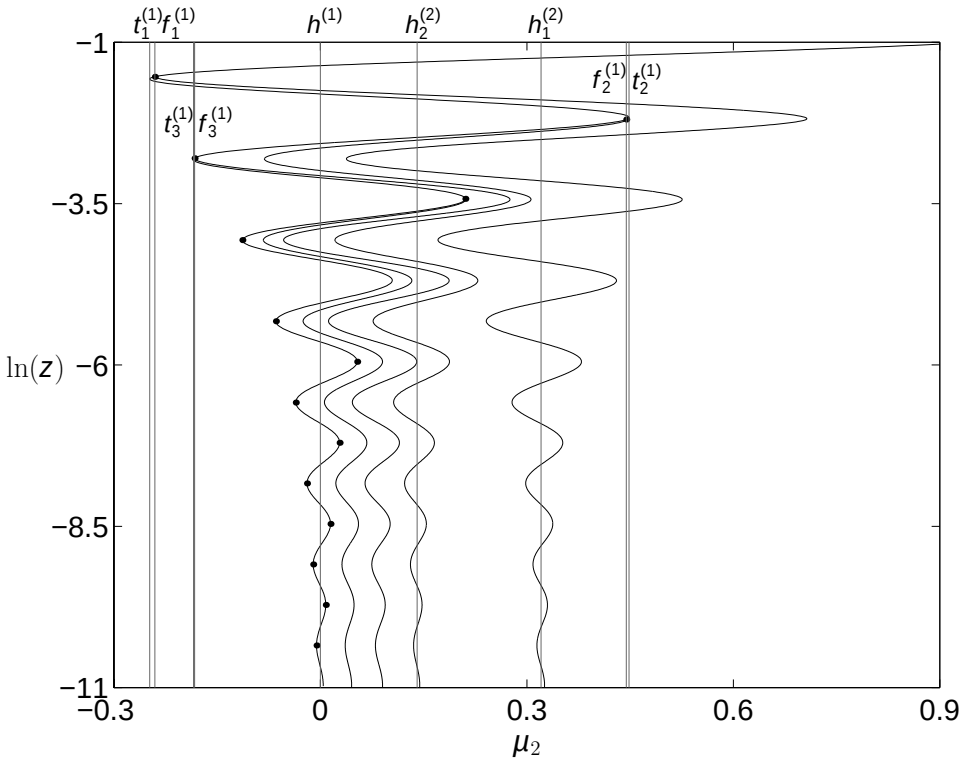

FIG. A.4. *One-parameter continuation of the fixed point and period-2 cycles of the normal form (A.8) for* $\mu_1 = 1, B = 1, \rho = \frac{1}{2}, \lambda = \frac{1}{5}$.

A.5. Bifurcations in a transversal one-parameter family. To get more insight into possible bifurcations near the Belyakov point, consider bifurcations of fixed points and cycles in the normal form (A.8), under variation of μ_2 with fixed $\mu_1 > 0$. This corresponds to bifurcations in a one-parameter family of systems (A.1) transversal to the saddle-focus homoclinic branch of $h^{(1)}$. FIG. A.4, obtained numerically using CONTENT [32], shows such bifurcations.

In the figure, a "wiggly" curve, originating in the upper right corner and approaching the line $\mu_2 = 0$, is the branch of fixed points of (A.8). Each turning point on this curve gives a tangent bifurcation (i.e., collision of two fixed points). The critical parameter values corresponding to the tangent bifurcations $t_n^{(1)}$ clearly accumulate on $\mu_2 = 0$ from both sides. As is predicted by the theory, very close to each turning point there exists a period-doubling bifurcation $f_n^{(1)}$. These points have dot markers in the figure. The corresponding parameter values also accumulate on $\mu_2 = 0$ from both sides. The numerical continuation of period-2 cycles bifurcating from the flip points shows that these cycles approach some values of $\mu_2 > 0$ as $z \to 0$ ($\ln z \to -\infty$). These values correspond to the double homoclinic bifurcations $h_n^{(2)}$ and accumulate on $\mu_2 = 0$ from the right ($\mu_2 > 0$). Notice that only a point with the minimal z-value on the period-2 cycle is plotted. The period-2 branches do not intersect and there is one double homoclinic bifurcation $h_n^{(2)}$ between each two tangent bifurcations $t_n^{(1)}$ and $t_{n+2}^{(1)}$. There are also sequences of tangent and flip bifurcations of period-2 cycles, accumulating on each double homoclinic bifurcation curve, etc.

REFERENCES

[1] V. Arnold, *Geometrical Methods in the Theory of Ordinary Differential Equations*, Springer-Verlag, New York, Heidelberg, Berlin, 1983.

[2] A. Bazykin, *Nonlinear Dynamics of Interacting Populations*, World Scientific Publishing Co. Inc., River Edge, NJ, 1998.

[3] L. Belyakov, *The bifurcation set in a system with a homoclinic saddle curve*, Mat. Zametki, 28 (1981), pp. 910–916.

[4] M. Boer, B. Kooi, and S. Kooijman, *Food chain dynamics in the chemostat*, Math. Biosci., 150 (1998), pp. 43–62.

[5] ———, *Homoclinic and heteroclinic orbits in a tri-trophic food chain*, J. Math. Biol., 39 (1999), pp. 19–38.

[6] A. Champneys and Y. Kuznetsov, *Numerical detection and continuation of codimension-two homoclinic bifurcations*, Int. J. Bifur. Chaos Appl. Sci. Engrg., 4 (1994), pp. 795–822.

[7] A. Champneys, Y. Kuznetsov, and B. Sandstede, *A numerical toolbox for homoclinic bifurcation analysis*, Int. J. Bifur. Chaos Appl. Sci. Engrg., 6 (1996), pp. 867–887.

[8] T. Chay, *Chaos in a three variable model of an excitable cell*, Physica D, 16 (1985), pp. 233–242.

[9] K. Cheng, *Uniqueness of a limit cycle of a predator-prey system*, SIAM J. Math. Anal., 12 (1981), pp. 541–548.

[10] O. De Feo, G. M. Maggio, and M. P. Kennedy, *The colpitts oscillator: Families of periodic solutions and their bifurcations*, Int. J. Bifur. Chaos Appl. Sci. Engrg., 10 (2000), pp. 935–958.

[11] O. De Feo and S. Rinaldi, *Yield and dynamics of tritrophic food chains*, Am. Nat., 150 (1997), pp. 328–345.

[12] ———, *Singular homoclinic bifurcations in tri-trophic food chains*, Math. Biosci., 148 (1998), pp. 7–20.

[13] O. Decroly and A. Goldbeter, *From simple to complex oscillatory behaviour: Analysis of bursting in a multiply regulated biochemical system*, J. Theor. Biol., 124 (1987), pp. 219–250.

[14] E. Doedel, A. Champneys, T. Fairgrieve, Y. Kuznetsov, B. Sandstede, and X. Wang, auto97*: Continuation and bifurcation software for ordinary differential equations (with* homcont). Computer Science, Concordia University, Montreal, Canada, 1997.

[15] J. Evans, N. Fenichel, and J. Feroe, *Double impulse solutions in nerve axon equations*, SIAM J. Appl. Math., 42 (1982), pp. 219–234.

[16] G. Feichtinger, C. Forst, and C. Piccardi, *A nonlinear dynamical model for the dynastic cycle*, Chaos, Solitons and Fractals, 7 (1996), pp. 257–271.

[17] H. Freedman and J. So, *Global stability and persistence of simple food chains*, Math. Biosci., 76 (1985), pp. 69–86.

[18] H. Freedman and P. Waltman, *Mathematical analysis of some three-species food-chain models*, Math. Biosci., 33 (1977), pp. 257–276.

[19] T. Gard, *Persistence in food chains with general interactions*, Math. Biosci., 51 (1980), pp. 165–174.

[20] P. Gaspard, R. Kapral, and G. Nicolis, *Bifurcation phenomena near homoclinic systems: A two-parameter analysis*, J. Stat. Phys., 35 (1984), pp. 697–727.

[21] P. Glendinning and C. Sparrow, *Local and global behaviour near homoclinic orbits*, J. Stat. Phys., 35 (1984), pp. 645–696.

[22] S. Gonchenko, D. Turaev, P. Gaspard, and G. Nicolis, *Complexity in the bifurcation structure of homoclinic loops to a saddle-focus*, Nonlinearity, 10 (1997), pp. 409–423.

[23] A. Gragnani, O. De Feo, and S. Rinaldi, *Food chains in the chemostat: relationships between mean yield and complex dynamics*, Bull. Math. Biol., 1 (1998), pp. 1–16.

[24] A. Hastings and T. Powell, *Chaos in a three-species food chain*, Ecol., 72 (1991), pp. 896–903.

[25] P. Hogeweg and B. Hesper, *Interactive instruction on population interactions*, Comp. Biol. Med., 8 (1978), pp. 319–327.

[26] M. Kærn and A. Hunding, *The effect of slow allosteric transitions in a coupled biochemical oscillator model*, J. Theor. Biol., 198 (1999), pp. 269–281.

[27] A. Khibnik, Y. Kuznetsov, V. Levitin, and E. Nikolaev, *Continuation techniques and interactive software for bifurcation analysis of ODEs and iterated maps*, Physica D, 62 (1993), pp. 360–371.

[28] A. Klebanoff and A. Hastings, *Chaos in three species food chains*, J. Math. Biol., 32 (1994), pp. 427–451.

[29] B. Kooi, M. Boer, and S. Kooijman, *Complex dynamic behaviour of autonomous microbial food chains*, J. Math. Biol., 36 (1997), pp. 24–40.

[30] ———, *Consequences of population models on the dynamics of food chains*, Math. Biosci., 153 (1998), pp. 99–124.

[31] Y. Kuznetsov, *Elements of Applied Bifurcation Theory*, Springer-Verlag, New York, Berlin, Heidelberg, 1995, 1998.

[32] Y. Kuznetsov and V. Levitin, CONTENT*: Integrated environment for the analysis of dynamical systems.* Centrum voor Wiskunde en Informatica, Amsterdam, The Netherlands, `ftp://ftp.cwi.nl/pub/CONTENT`, 1997.

[33] Y. Kuznetsov and S. Rinaldi, *Remarks on food chain dynamics*, Math. Biosci., 134 (1996), pp. 1–33.

[34] A. Lotka, *Elements of Physical Biology*, Williams and Wilkins, Baltimore, MD, 1925.

[35] R. May, *Limit cycles in predator-prey communities*, Science, 177 (1972), pp. 900–902.

[36] K. McCann and P. Yodzis, *Biological conditions for chaos in a three-species food chain*, Ecol., 75 (1994), pp. 561–564.

[37] ———, *Bifurcation structure of a three-species food chain model*, Theor. Pop. Biol., 48 (1995), pp. 93–125.

[38] S. Muratori and S. Rinaldi, *A separation condition for the existence of limit cycles in slow-fast systems*, Appl. Math. Modelling, 15 (1991), pp. 312–318.

[39] ———, *Low- and high-frequency oscillations in three-dimensional food chain systems*, SIAM J. Appl. Math., 52 (1992), pp. 1688–1706.

[40] S. Rinaldi, S. Dal Bo, and E. De Nittis, *On the role of body size in a tri-trophic metapopulation model*, J. Math. Biol., 35 (1996), pp. 158–176.

[41] A. Sherman, J. Rinzer, and J. Keuzer, *Emergence of organized bursting in clusters of pancreaic α-cells by channel sharing*, Biophys. J., 54 (1988), pp. 411–425.

[42] V. Volterra, *Variazioni e fluttuazioni del numero di individui in specie animali conviventi*, Mem. Accad. Lincei, 2 (1926), pp. 31–113. (In Italian).